International Journal of Remote Sensing
Vol. 29, No. 2, 20 January 2008, 513–527

Taylor & Francis
Taylor & Francis Group

An experimental evaluation of non-rigid registration techniques on Quickbird satellite imagery

V. ARÉVALO* and J. GONZÁLEZ
Department of System Engineering and Automation, University of Málaga, Campus Teatinos, 29071, Málaga, Spain

(*Received 26 June 2006; in final form 20 November 2006*)

In remote sensing, because of the wide diversity of image characteristics (size, spatial and radiometric resolution, terrain relief, observation poses, etc.), image registration methods that work well on certain satellite images may not produce acceptable results for others, requiring more powerful techniques. A variety of registration techniques that account for images with non-rigid geometric deformations have been proposed, including piecewise (linear or cubic) functions, weighted mean functions, radial basis functions, B-spline functions, etc. This paper compares three of them: polynomial, piecewise-linear and thin-plate-spline functions, and analyses their performance under a variety of factors: off-nadir viewing, terrain relief, density of control points, and 3D geometric correction. Our comparison applies on panchromatic QuickBird imagery, both ortho-ready (as provided by DigitalGlobe) and orthorectified, acquired on different dates, from different observation attitudes, and sensing different land covers: urban area, high-relief terrain, and a combination of both.

1. Introduction

Image registration is the process of spatially aligning two or more images of the same scene acquired on different dates (multitemporal analysis), from different viewpoints (multiview analysis) and/or using different sensors (multimodal analysis). In this process, one image remains without modification (the fixed image), whereas the other (the moving image) is transformed until fitting with the fixed one. Image registration is a necessary step in those image-analysis applications where the final result comes from the association of several data sources, for example, image fusion, change detection, 3D scene reconstruction, etc.

In remote sensing, because of the wide range of image characteristics (size, spatial and radiometric resolution, sensed scene, observation pose, etc.), one registration method that may work well on certain satellite images will not produce acceptable results for others, requiring more powerful techniques. To be specific, global polynomial functions usually perform well with low- and medium-resolution images (Landsat, IRS, Spot, etc.) but may not be effective enough to register high-resolution images such as QuickBird, Ikonos, or OrbView. The main reasons for the limited performance include (figure 1):

1. Larger image distortions because of the higher resolution. Distortion comes from different sources, but the most significant one is the off-nadir

*Corresponding author. Email: varevalo@ctima.uma.es

International Journal of Remote Sensing
ISSN 0143-1161 print/ISSN 1366-5901 online © 2008 Taylor & Francis
http://www.tandf.co.uk/journals
DOI: 10.1080/01431160701241910

Figure 1. Pair of QuickBird satellite images of the same scene taken from different observation angles. Note the geometric and radiometric differences between both images. Available in colour online.

observation angle. For offering shorter revisit periods, these satellites can observe the scene from very different paths and angles, which gives rise to images with significant non-rigid geometric differences.

2. Changes in the scene (even small changes) now appear clearer in the images, and so it is more difficult to successfully accomplish some stages of the registration process like detecting corresponding points or measuring the registration goodness. Examples of these changes include temporal changes, cast shadows, different sides of a building, etc.

To address the registration of images with high relative distortions some elastic fitting methods have been proposed in the image-processing literature, including: piecewise linear (Goshtasby 1986, Sheng and Alsdorf 2005) or cubic (Goshtasby 1987) functions, multiquadric functions (Ehlers and Fogel 1994), radial basis functions (Bookstein 1989), B-spline functions (Kybic and Unser 2003), etc. These techniques can be grouped into any of the following approaches:

1. *Intensity-based methods*, where registration is approached as an optimization process in which a cost function based on the radiometric similarity of both images is maximized.
2. *Landmark-based methods*, that transform the moving image by a mapping function estimated from a set of representative pairs of control points (also called landmarks) identified in both images.

Most of the elastic registration techniques applied within the remote-sensing field follow this second approach since they are more efficient computationally. Despite that, landmark-based methods may require a considerable amount of time to identify precise corresponding points in both images, which may become a serious problem in many practical situations where hundreds of control points are needed for capturing the relative geometric distortions. From a user's point of view, it is clear that if a simple registration method (i.e. global polynomial function) achieves the accuracy required for a particular application, there is no need to waste time clicking extra control points demanded by a more powerful technique.

Thus, we are interested in knowing the performance of these techniques on high-resolution QuickBird satellite images and in which cases more sophisticated registration procedures become necessary. To this aim, this paper compares three representative landmark-based registration methods (all of them are included in

most of the current commercial satellite image-processing packages, such as ERDAS, ENVI, and PCI): polynomial, piecewise-linear, and thin-plate-spline functions under a variety of acquisition factors that influence their performance (e.g. off-nadir viewing, terrain relief, etc.). This work also analyses the influence of an image orthorectification process on the analysed methods by contrasting the experimental results achieved with both standard (ortho-ready products) and orthorectified imagery. In particular, our comparison focuses on panchromatic QuickBird images (0.6 m per pixel) acquired on different dates, from different viewpoints, and sensing different terrain profiles. For measuring the registration consistency, we consider two metrics: root mean square error (RMSE) and circular error with 90% confidence (CE90).

The remainder of this paper is organized as follows. In §2, we review the non-rigid registration techniques considered in this study. In §3, the datasets (images and sets of corresponding points) and the metrics for measuring the registration consistency in the comparison are described. In §4, we present and discuss the experimental results. Finally, some conclusions and future work are outlined.

2. Image registration methods

Landmark-based registration is usually carried out in three stages (Zitová and Flusser 2003). In the first, the positions of a set of pairs of control points (CP) are accurately identified in the fixed and moving images; in the second, this set of CP is used to estimate a geometric transformation function between both images; finally in the third, the moving image is spatially transformed to overlap the fixed image using the estimated mapping function and by applying some interpolation techniques such as nearest neighbour, bilinear, bicubic, or splines. For the registration to be successful, (1) the correspondence pairs must be distributed on the images according to their geometric differences, and (2) the applied transformation must be powerful enough to cope with the (possibly non-rigid) distortions.

As mentioned previously, this paper evaluates three well-known methods of image registration and analyses their performance on QuickBird imagery. More precisely, we have compared a *global* procedure based on polynomial functions (of diverse orders), a *local* method based on piecewise-linear functions, and a *hybrid* technique based on radial basis functions (concretely, thin-plate splines (TPS)). Formally, a pair of generic image mapping functions can be expressed as follows:

$$\begin{aligned} x &= f_x(x', y') \\ y &= f_y(x', y'), \end{aligned} \tag{1}$$

where (x, y) and (x', y') are the CP coordinates in the fixed and moving images, respectively.

In the next subsections, the mapping functions applied in this work are described. For a more detailed analysis of these techniques in terms of their computational complexity, the reader may refer to Image Fusion Systems Research (2003).

2.1 *Polynomial functions*

Polynomial functions have been broadly used in remote sensing to register low- and medium-resolution images (Landsat, IRS, Spot, etc.) and thematic data (Novak 1992, Estrada *et al.* 2000). The kind of geometric differences that these functions can

manage depends on the polynomial order. Thus, we can use first-order transformations to model translations, rotations and scale changes, that is, *rigid* distortions and second- and higher orders to model more complex distortions, named *non-rigid* or *elastic* distortions. A pair of polynomial functions of order t are defined as follows:

$$x = f_x(x', y') = \sum_{i=0}^{t} \sum_{j=0}^{i} a_{ij} (x')^{i-j} (y')^j \tag{2}$$

$$y = f_y(x', y') = \sum_{i=0}^{t} \sum_{j=0}^{i} b_{ij} (x')^{i-j} (y')^j, \tag{3}$$

where a_{ij} and b_{ij} are the polynomial coefficients.

The order of the polynomial also determines the minimum number of CP to be estimated. For example, to estimate a first-order transformation, three non-collinear points are required. The following expression provides the minimum number N of CP required to estimate a polynomial function of order t:

$$N = \frac{(t+1)(t+2)}{2}. \tag{4}$$

In practice, since the number of CPs is usually higher than N, the coefficients are computed by means of a least-squares fitting, so that the polynomials minimize the sum of squared errors at the CPs.

The limitation of this transformation comes from its global scope which allows us to cope with important image differences, but only if they are spread over the whole image following the assumed polynomial model (figure 2(*a*)).

2.2 *Piecewise-linear functions*

Piecewise-linear functions deal with the registration process by dividing the images in triangular elements (for example, by Delaunay's triangulation method) which are then individually mapped through a linear transformation (Goshtasby 1986). Although this approach guarantees the continuity of adjacent triangles, it does not produce smooth transitions between them, which may cause an undesirable visual effect in the transformed image (i.e. line segments are not preserved). A pair of piecewise-linear functions are defined as:

$$\begin{aligned} x = f_x(x', y') &= \begin{cases} a_{11} + a_{12}x' + a_{13}y' & \text{if} \quad (x', y') \in t_1 \\ \quad\vdots \\ a_{n1} + a_{n2}x' + a_{n3}y' & \text{if} \quad (x', y') \in t_n \end{cases} \\ y = f_y(x', y') &= \begin{cases} b_{11} + b_{12}x' + b_{13}y' & \text{if} \quad (x', y') \in t_1 \\ \quad\vdots \\ b_{n1} + b_{n2}x' + b_{n3}y' & \text{if} \quad (x', y') \in t_n, \end{cases} \end{aligned} \tag{5}$$

where t_i is a triangular element built upon three CPs (provided by the triangulation method); a_{ij} and b_{ij} with j=1, 2, 3 are the polynomial coefficients of the linear

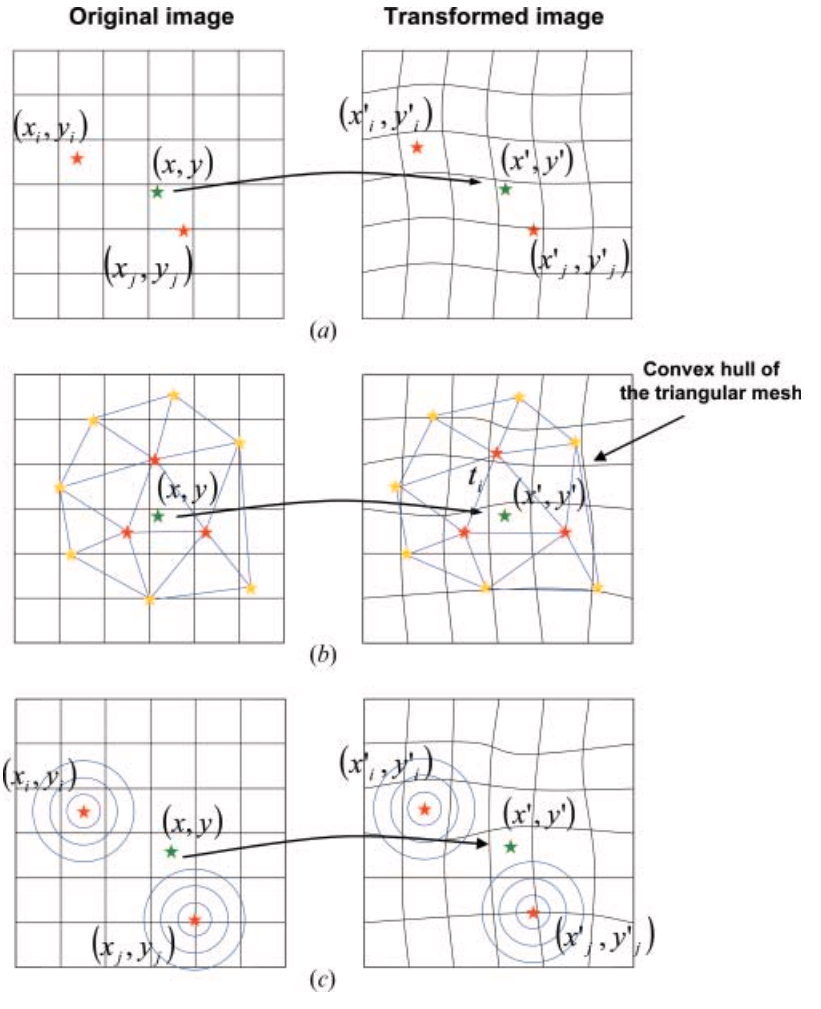

Figure 2. Different mapping functions considered in this paper: (*a*) polynomial, (*b*) piecewise-linear, and (c) thin-plate-spline.

functions corresponding to the triangle t_i; and n is the number of triangular elements.

In general, the number of CPs required for a good registration will depend on the type of deformation to be modelled in the image, ranging from several dozen to thousands. Notice that, the mapping functions are only defined inside the convex hull of the control point set. Although it is possible to extrapolate these functions outside this region, we do not consider that option in this work because it would introduce an extra error that could distort the registration result (figure 2(*b*)).

2.3 *Radial basis functions (TPS functions)*

Radial basis functions (RBF) are scattered data interpolation methods where the spatial transformation is a linear combination of radially symmetric basis functions, each of them centred on a particular CP. RBFs provide smooth deformations with easily controllable behaviour (figure 2(*c*)). In two dimensions, an RBF consists of

two mapping functions that comprise a global component (typically, an affine transformation) and a local component. Given n corresponding CPs, we can define a pair of radial basis functions as follows:

$$x = f_x(x', y') = \sum_{i=0}^{t} \sum_{j=0}^{i} a_{ij} (x')^{i-j} (y')^{j} + \sum_{i=1}^{n} A_i g(r_i) \tag{6}$$

$$y = f_y(x', y') = \sum_{i=0}^{t} \sum_{j=0}^{i} b_{ij} (x')^{i-j} (y')^{j} + \sum_{i=1}^{n} B_i g(r_i), \tag{7}$$

where a_{ij} and b_{ij} are the coefficients of a polynomial of order t (global component); A_i and B_i are the coefficients of a linear combination of radially symmetric functions $g(r_i)$ (the basis functions), where r_i denotes the Euclidean norm, that is

$$r_i = \left\| (x', y') - (x'_i, y'_i) \right\| = \sqrt{(x' - x'_i)^2 + (y' - y'_i)^2}. \tag{8}$$

The type of basis function determines the influence of each CP on the RBF, that is, the CP scope. Some RBFs have a global behaviour (e.g. TPS), whereas others have a more local influence (e.g. Gaussians). Table 1 shows some commonly used RBFs.

In particular, in this paper we are interested in the behaviour of TPS functions, which is perhaps the transformation most widely employed for elastic registration. TPS was introduced by Harder and Desmarais (1972) and successfully applied to register Landsat (Goshtasby 1988) and medical images (Bookstein 1989).

3. Datasets and metrics

The goal of this work is to evaluate the performance of the elastic mapping functions mentioned previously regarding the following three issues:

1. How they model the nonlinear deformations that arise in a pair of QuickBird images because of the terrain relief and off-nadir observation angle.
2. To what extent a basic orthorectification of the image (just using a DEM, no GCPs) minimizes the terrain and off-nadir viewing effects.
3. How the number of CPs influences the registration accuracy.

For this purpose, we consider a variety of dataset (images and sets of CP) and two metrics of image registration consistency which are described in the following sections.

Table 1. Types of radial basis functions (RFB).

Basis function	$g(r_i)$	Parameters	Scope
Thin-plate spline	$r_i^2 \log r_i^2$	–	Global
Multi-quadric	$\left(r_i^2 + \delta\right)^{\pm\mu}$	$\delta>0$, $\mu\neq0$	Local
Gaussian	$e^{\left(-r_i^2/\sigma\right)}$	$\delta>0$	Local
Shifted-LOG	$\log\left(r_i^2 + \delta\right)^{\frac{3}{2}}$	$\delta\geqslant0$	Local
Cubic spline	$\|r_i\|^3$	–	Global

3.1 *Datasets*

In this section, we give a brief description of the test images as well as the CP sets used in this study.

3.1.1 Test images. We have considered three images (QuickBird Ortho-Ready products) of the city of Rincón de la Victoria (Málaga-Spain) acquired on different dates, from different poses and covering different terrain profiles: urban area (which is almost plain) and mountainous area (high relief). Figure 3(*a*) shows two of these test images where the regions of interest are marked. To delimit such regions, we have made use of the elevation contours plotted on figure 3(*b*). The plot on top of the figure 3(*a*) shows a terrain profile along the arrow in the right image (from the mountains to the coastline) where altitude levels range from 300 m to 0 m. This elevation information has been obtained from a DEM with a spatial resolution of 20×20 m (this is the most accurate DEM available currently for the area) provided by the 'Consejería de Medio Ambiente' of the 'Junta de Andalucía'.

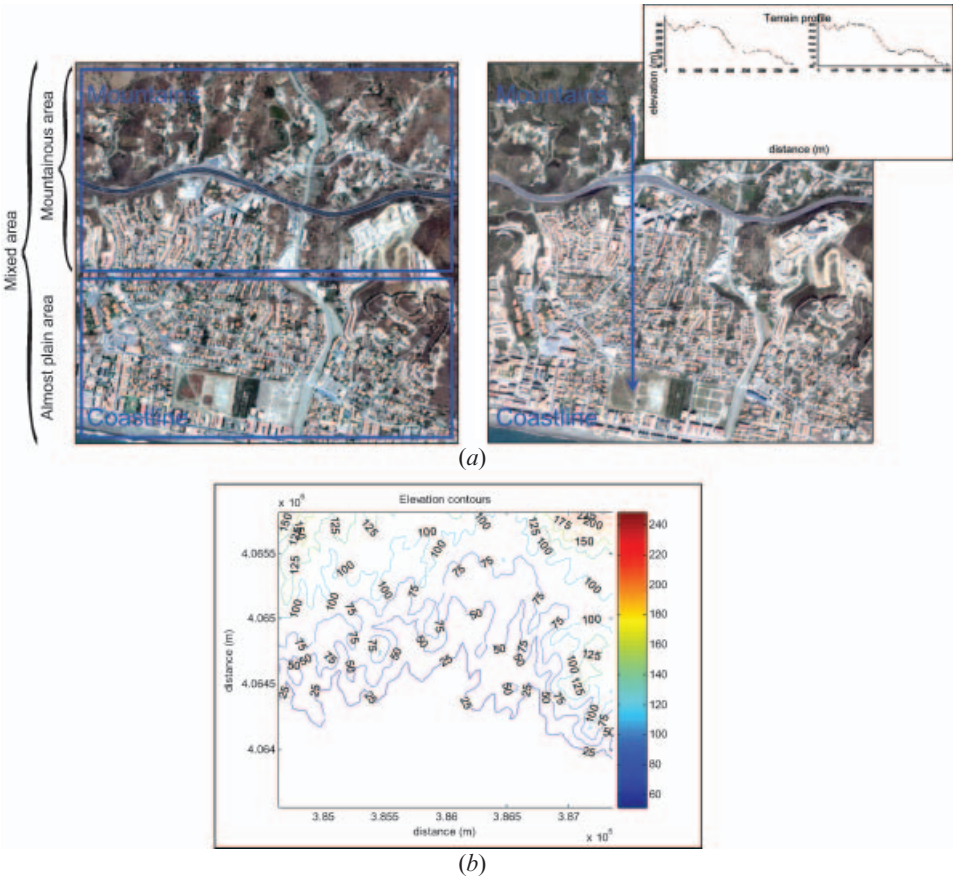

Figure 3. (*a*) Two test images of the city of Rincón de la Victoria (Málaga-Spain). These images cover approximately 4 km^2 and contain all different zones of interest for the comparison tests (mountains, city, and coast). The plot on top shows graphically a terrain profile of such region. (*b*) Elevation information considered to properly define the regions of interest: almost plain and high-relief areas.

Table 2. Positioning data (°) for the images used in the tests (refer to figure 4 for the meanings of these angles).

Angles	Image 1 (i1)	Image 2 (i2)	Image 3 (i3)
In track	15.9	−12.8	−1.1
Cross-track	10.8	−2.3	11.0
Off nadir	19.3	12.8	10.9

Table 2 shows the QuickBird viewing direction for the images used in the experiments. The pairs considered for registration are {<i1–i2>, <i1–i3>, <i2–i3>}. These image pairs have different relative observation angles which, in combination with the terrain relief (the same for all the images), give rise to diverse geometric distortions (figure 4).

On the other hand, with the aim of analysing the influence of the orthorectification process in the image registration, we have also considered the same set of pairs of images after being orthorectified. The orthorectification of the three images was performed through the ERDAS implementation of the RPC method with the above-mentioned DEM and with no GCPs. This method has recently gained popularity due to the release of satellites such as QuickBird or Ikonos, which do not provide satellite-sensor information. Instead, they provide the coefficients of the rational polynomials (RPC files) required for a simplified camera projection model (developed by DigitalGlobe®), which approximates the 3D rigorous physical model (Toutin and Cheng 2002).

3.1.2 Control point sets. Two different sets of matched points are required: control points (CP) to estimate the coefficients of the mapping functions and independent checkpoints (ICP) to evaluate the accuracy of the registration. To guarantee a uniform distribution of them over the image, we select a point from every cell of a

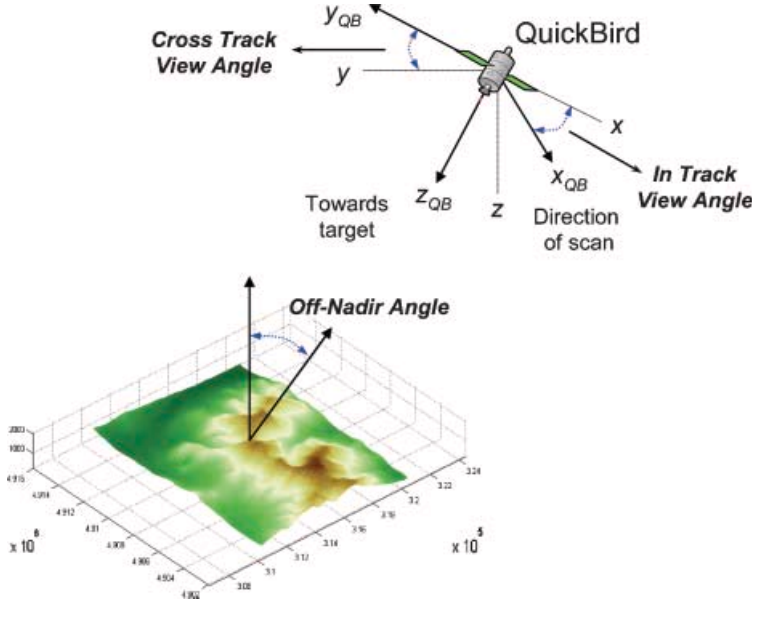

Figure 4. Satellite observation geometry. Available in colour online.

rectangular grid. In order to have different densities of control points, we define a variety of cell widths: 50 pixels for the ICP set and 100, 200, and 400 pixels for the CP sets. For 0.6-m-resolution QuickBird images, these sizes correspond to 30, 60, 120, and 240 m, respectively (figure 3); in other words, we dispose of three sets of 900, 225, and 64 CPs, and one set of 3600 ICPs for each pair of images. Apart from this set of points that allows us to study a mountainous and urban area together (mixed area), we also consider the subregions of interest marked in figure 3(*a*), obtaining two subsets, one for the mountainous area and another for the urban area. Thus, when analysing a particular area, we make use of its associated subset of CP and ICP.

To accurately identify these CP and ICP pairs, we have applied an automatic procedure based on the following techniques:

1. the Harris detector (Harris and Stephens 1988) to identify distinctive feature points in the fixed image; and
2. the Lucas–Kanade point tracker (Lucas and Kanade 1981) to detect their corresponding points in the morning image. This technique provides subpixel accuracy, as reported in Bouguet (1999) and works well when both images are roughly aligned, which was done manually.

Next, the affine epipolar geometry of the two images (concretely, the affine fundamental matrix) is robustly estimated, and the outliers (CPs not consistent with the estimated geometry) are removed from the initial set of point correspondences (Hartley and Zisserman 2003). Typically, several point pairs are obtained for each cell of the grid, but we only chose one: that with the more 'similar' neighbourhood (the similarity function considered in this work is the normalized cross-correlation). This process ensures a uniform distribution of control points throughout the image (figure 5).

It is important to remark that although this automatic procedure allows us to manage a large number of consistently matched point pairs (both CP and ICP), it does not guarantee that the corresponding points are the most suitable ones to capture the goodness of the image registration. For example, a perfectly matched ICP pair lying on a flat roof of a very tall building is not appropriate for measuring

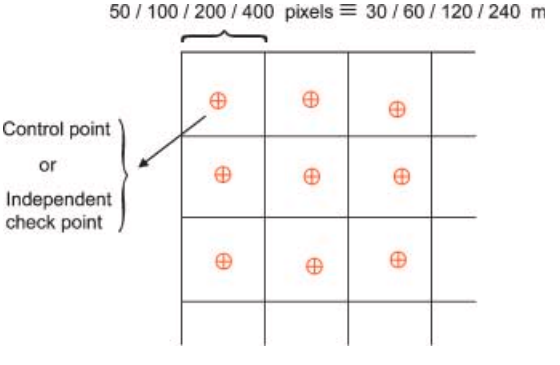

Figure 5. Procedure followed to spread both CPs and ICPs on the image. We divide it into a grid and choose one single point from each cell. The cell sizes used in this work are 50 pixels for the ICP set and 100, 200, and 400 pixels for the CP sets (for QuickBird images, these widths correspond to 30, 60, 120, and 240 m, respectively).

how good the ground or small buildings have been registered. This problem shows up in some of the experimental results in §4.

3.2 *Metrics for registration consistency*

To evaluate the precision of each method, the following two metrics are utilized: circular error with 90% confidence (CE90) and root mean square error (RMSE). Both measures are applied to the registration errors of the ICP pairs, which are computed from the distances between corresponding ICPs of the fixed and registered images.

3.2.1 Circular error with 90% confidence. The CE90 is a metric to describe the accuracy in map or image products at the 90% confidence level, that is, 90% of the ICP pairs must have distance errors within a circle of radius CE90. From a statistical point of view, this is stated in terms of the probability P such that:

$$P(\|(\hat{x}, \hat{y}) - (x, y)\| \leq \text{CE90}) = 90\%,$$

where (x, y) and $(\hat{x}, \hat{y})$ are the pixel coordinates of the fixed image ICP and of its corresponding ICP in the registered image.

3.2.2 Root mean square error. The RMS is also a metric to describe the accuracy of a registration process by measuring the magnitude of the average distance error, which is computed as the square root of the mean of the squares of the errors associated to each ICP pair. It is mathematically computed from:

$$\text{RMSE} = \sqrt{\frac{1}{n}\sum_{i=1}^{n} \|(\hat{x}, \hat{y}) - (x, y)\|^2}, \tag{9}$$

where n is the number of ICPs, and (x, y) and $(\hat{x}, \hat{y})$ are the ICP coordinates (as defined above).

RMSE and CE90 are two complementary metrics commonly used in remote sensing. The main difference between them is that RMSE takes into account errors from all the pairs, including those that could be considered outlier matches. On the contrary, CE90 is only affected by the majority of them (the 90%), not capturing how bad the remaining 10% are.

4. Experiments and results

In this section, the performances of the polynomial (from the second to the sixth order), piecewise-linear, and thin-plate-spline functions (with affine global components) are compared for different numbers of CPs, terrain profiles, and observation angles. Since the effect of any of these parameters on the registration accuracy depends on the values of the others, an exhaustive analysis of them requires trials over all the possible combinations. We have carried out all these tests, though here we only show the comparative plots for those that we understand are of more significance. Regarding the estimate of the mapping coefficients, they have been computed by means of software written in C++ which takes advantage of *The OpenCV Library* primitives. The Open Source Computer Vision Library is a collection of algorithms and sample code for various computer vision problems. The library is compatible with IPL and utilizes Intel® Integrated Performance Primitives

for better performance. Visit http://www.sourceforge.net/projects/opencvlibrary for further information. Two points must also be highlighted:

- We have experimentally verified that polynomials of an order higher than fourth order barely improve the registration, although they require many more CPs to be estimated. Consequently, we only show results for the fourth-order one, which requires a minimum of 15 CPs.
- As reported in the literature (Madych 1992), when the number of control points is high (e.g. more than 1000), the equation system to be solved for the thin-plate-spline functions becomes ill-conditioned. To overcome this problem, we have implemented the iterative method proposed in Beatson *et al.* (2001).

Figure 6(*a*) shows the influence of the *number of control points* (i.e. their density) in each method. In these charts, we have fixed the angle of observation (image pair <i1–i2> which has the largest difference angle) and the terrain relief (mixed). The most interesting conclusion from it is that local methods (PWL and TPS) take advantage of the number of points, achieving very accurate results for the dense CP

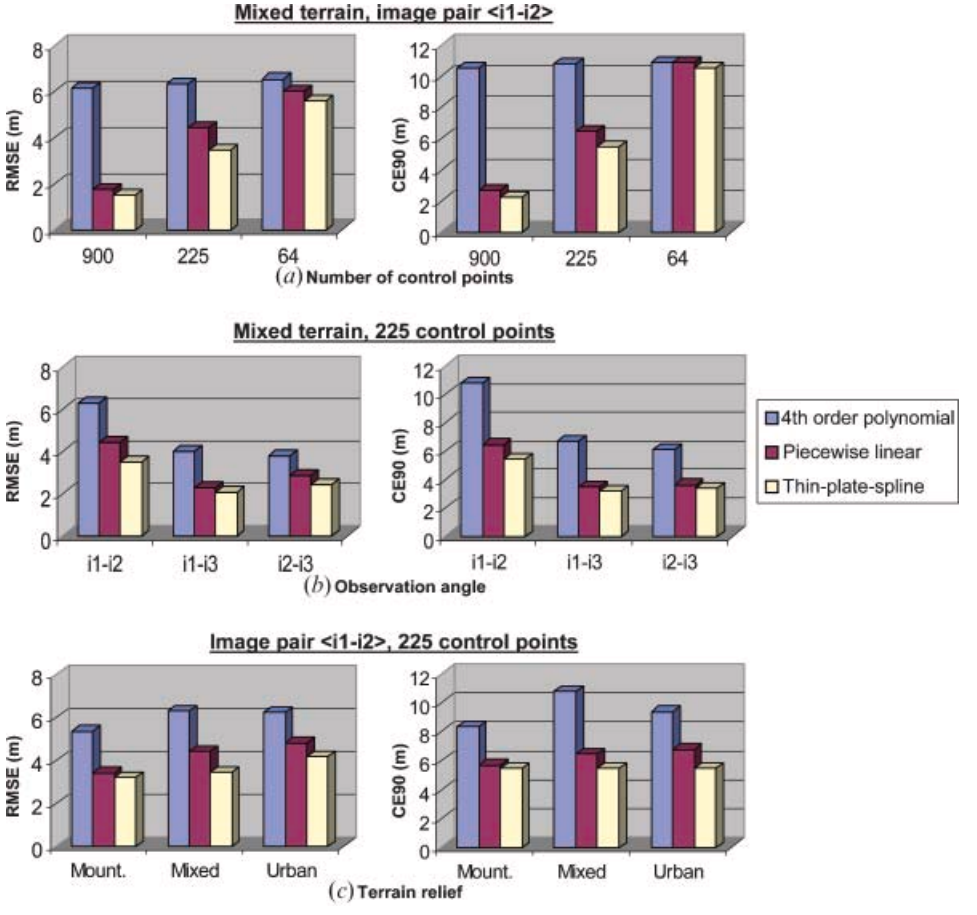

Figure 6. RMSE and CE90 values for elastic functions analysed in this work according to: (*a*) number of CPs, (*b*) angle of observation (image pairs), and (*c*) terrain relief. Above each row are the fixed values of the other parameters.

set (about 1.75 m RMSE); on the contrary, global functions (POL4) do not improve the performance for a higher number of points since nothing (except robustness) is gained when more than the required 15 CPs are employed. Notice also that when the number of CPs decreases (sparse CP sets), local transformations become global (weak local) and cannot adapt well to the local geometric differences between images.

Figure 6(*b*) shows the influence of the *angle of observation* for a mixed terrain and 225 CPs (taken from cells of 120 m width). From this comparison, we can observe that all methods (local and global) are sensitive to the angle of observation though the influence is greater for the POL4 global method. Although not shown here, for a denser set of CPs, POL4 performs similarly (practically not an improvement of the results of figure 6(*b*)), while the local methods achieve better results, especially for the pair <i1–i2>.

The effect of the *terrain relief* is displayed in figure 6(*c*), where we can highlight two things: (1) local methods perform very similar in all profiles, (2) the polynomial function (POL4) works worse on mixed terrain, which makes sense, since it cannot fit well different deformation models simultaneously. Figure 7 (which also contains figure 6(*c*)) is a more comprehensive chart aimed to give us, at a single glance, the increasing effect of the observation angle for more irregular terrains (relative viewing angles of <i1–i3> and <i2–i3> are very similar). Notice that the estimated registration error for the urban area is significantly greater than for the mountains. We attribute this result to: (1) the existence, as commented earlier in §3.1.2, of an important portion of ICPs that lie on top of the buildings; and (2) the elevation levels of the urban area is not negligible, as revealed later, once the orthorectification process is accomplished.

Finally, the effects of using orthorectified images are shown in figure 8. Similarly to figure 7, this chart illustrates the influence of the terrain relief in combination with the observation angle. As we can see, a certain correlation exists between both charts, but in this case, the performance of all methods is significantly improved, especially for the polynomial methods. In addition, we observe that the registration errors using the fourth-order polynomial function (POL4) on the orthorectified images are almost as good as those applying local methods over non-orthorectified

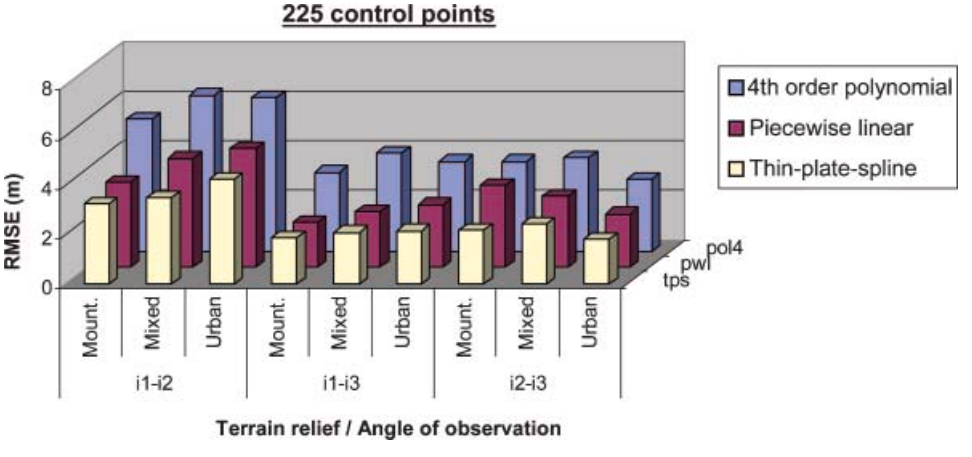

Figure 7. RMSE values for the considered functions grouped by the angle of observation and the terrain relief.

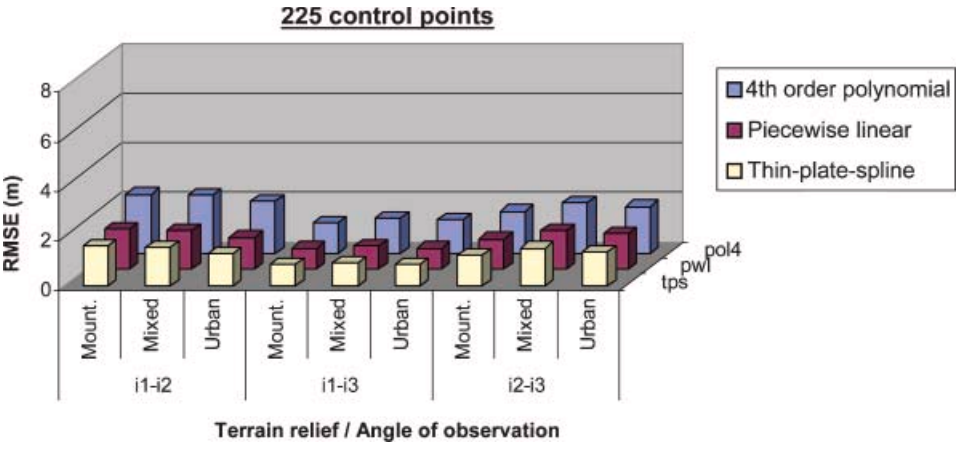

Figure 8. RMSE values for the considered functions grouped by the angle of observation and the terrain relief (in this case, the test images have been orthorectified).

methods, even though the number of CPs being used in both cases is quite different: 15 for the POL4 versus 225 for local methods. On the other hand, although the buildings are not orthorectified in this process, the errors for the urban area are significantly improved. From these results, we can conclude that such an area presents, unlike initially supposed, significant elevation differences. The explanation for this general improvement is that the image orthorectification compensates the local distortions induced by the terrain relief and the off-nadir viewing.

As mentioned in §2.2, piecewise-linear functions may cause a broken-line effect (at the triangle transitions) in the transformed image over the straight elements of the scene such as roads, buildings, etc. We have visually checked that this problem only becomes significant when the terrain profile varies substantially (i.e. in the mountainous area) and the coarser mesh generated from the sparse CP set (only 64 CPs for the entire image) is applied. In these cases, other registration methods such as piecewise cubic or TPS should be considered to avoid this effect.

In summarizing, from these experiments we can draw the following conclusions:

1. Local methods (particularly, TPS) present a better performance in all the experiments than the polynomial functions of fourth order. When using a local method, it is worth having as many points as possible (but not for global ones).
2. When the scene under observation contains elements at very different heights (i.e. mountains, high buildings, etc.) global methods are suitable for high-resolution image registration only in any of the following situations:

   a. both images have been acquired from very close viewing angles;
   b. images have been orthorectified (an RPC-based method with no GCP may suffice).

Thus, except for those cases where we certainly know that either the captured scene is practically plain, with no elements at different heights, or the two images have been taken with almost the same observation angle, we would suggest employing local methods with as many CPs as possible (the larger the number of

points, the better the registration accuracy). This result brings up the importance of developing an automatic and reliable procedure to find well-distributed pairs of CPs in the images. On the other hand, if we have a DEM available, RPC-based image orthorectification leads to a significant improvement in the registration, especially when using polynomial methods which need to identify fewer CPs than local methods.

5. Conclusions

High-resolution satellite images such as QuickBird are expected to play an important role in many remote-sensing applications. To achieving this, tools commonly used for lower-resolution images may not be appropriate, as is the case for traditional image-registration methods. This paper has experimentally analysed the performance of three well-known elastic registration techniques such as polynomial, piecewise-linear and TPS functions for diverse conditions: number of control points, terrain relief, acquisition angles, and image corrections (orthorectification). We have evaluated their suitability and accuracy for registering QuickBird images according to two metrics: root mean square error (RMSE) and circular error with 90% confidence (CE90).

From this analysis, we have verified some of the intuitions that we had, but more importantly, this has allowed us to quantify the influence of the above factors in the performance of each registration method. Using non-orthorectified images, local methods (PWL or TPS) beat by far the global one (POL4), since they can exploit the information provided by many CPs. However, when images to be registered are previously orthorectified (even not very precisely), our study has revealed that the polynomial adjustment yields good results, even for high-relief terrain and different viewing angles.

Acknowledgements

The authors would like to thank two reviewers whose comments have significantly improved the manuscript. The ©DigitalGlobe QuickBird imagery used in this study is distributed by Eurimage, SpA. (www.eurimage.com) and provided by Decasat Ingenieria S.L., Málaga, Spain (www.decasat.com). This work was supported by the Spanish Government under the research project CICYT-DPI2005-01391. A preliminary version of this paper was presented in the 'ISPRS Technical Commission VII, Mid Term Symposium 2006, Remote Sensing: From Pixels to Processes'.

References

BEATSON, R.K., LIGHT, W.A. and BILLINGS, S.D., 2001, Domain decomposition methods for solution of the radial basis function interpolation equations. *SIAM Journal on Scientific Computing*, **22**, pp. 1717–1740.

BOOKSTEIN, F., 1989, Principal warps: thin-plate splines and the decomposition of deformations. *IEEE Transactions on Pattern Analysis and Machine Intelligence*, **11**, pp. 567–585.

BOUGUET, J.Y., 1999, Pyramidal implementation of the Lucas–Kanade feature tracker. Description of the algorithm. *Intel Corporation, Microprocessor Research Labs*, OpenCV Documents. Available online at: http://robots.stanford.edu/cs223b04/algo_tracking.pdf (accessed 21 September 2006).

EHLERS, M. and FOGEL, D.N., 1994, High-precision geometric correction of airborne remote sensing revisited: the multiquadric interpolation. *Proceedings of SPIE: Image and Signal Processing for Remote Sensing*, **2315**, pp. 814–824.

ESTRADA, M., YAMAZAKI, F. and MATSUOKA, M., 2000, Use of LANDSAT images for the identification of damage due to the 1999 Kocaeli, Turkey Earthquake. In *Proceedings of the 21st Asian Conference on Remote Sensing*, Taipei, Taiwan.

GOSHTASBY, A., 1986, Piecewise linear mapping functions for image registration. *Pattern Recognition*, **19**, pp. 459–466.

GOSHTASBY, A., 1987, Piecewise cubic mapping functions for image registration. *Pattern Recognition*, **20**, pp. 525–533.

GOSHTASBY, A., 1988, Registration of images with geometric distortion. *IEEE Transactions on Geosciences and Remote Sensing*, **26**, pp. 60–64.

HARDER, R.L. and DESMARAIS, R.N., 1972, Interpolation using surface splines. *Journal of Aircraft*, **9**, pp. 189–191.

HARRIS, C.J. and STEPHENS, M., 1988, A combined corner and edge detector. In *Proceedings of the 4th Alvey Vision Conference*, Manchester, UK, pp. 147–151.

HARTLEY, R.I. and ZISSERMAN, A., 2003, *Multiple View Geometry in Computer Vision*, pp. 279–292 (Cambridge: Cambridge University Press).

IMAGE FUSION SYSTEMS RESEARCH, 2003, Transformation functions for image registration. In *IFSR Technical Report.* Available online at: http://www.imgfsr.com/ifsr_tf.pdf (accessed 21 September 2006).

KYBIC, J. and UNSER, M., 2003, Fast parametric elastic image registration. *IEEE Transactions on Image Processing*, **12**, pp. 1427–1442.

LUCAS, B.D. and KANADE, T., 1981, An iterative image registration technique with an application to stereo vision. In *International Joint Conference on Artificial Intelligence*, **81**, pp. 674–679.

MADYCH, W., 1992, Miscellaneous error bounds for multi-quadric and related interpolators. *Computers & Mathematics with Applications*, **24**, pp. 121–138.

NOVAK, K., 1992, Rectification of digital imagery. *Photogrammetric Engineering and Remote Sensing*, **58**, pp. 339–344.

SHENG, Y. and ALSDORF, D., 2005, Automated ortho-rectification of amazon basin-wide SAR mosaics using SRTM DEM data. *IEEE Transactions on Geoscience and Remote Sensing*, **43**, pp. 1929–1940.

TOUTIN, T. and CHENG, P., 2002, QuickBird—a milestone for high resolution mapping. *Earth Observation Magazine*, **11**, pp. 14–18.

ZITOVÁ, B. and FLUSSER, J., 2003, Image registration methods: a survey. *Image and Vision Computing*, **21**, pp. 977–1000.